Science Signaling
AAAS

www.sciencesignaling.org/cgi/content/full/7/339/ra78/DC1

Supplementary Materials for

The ErbB4 CYT2 variant protects EGFR from ligand-induced degradation to enhance cancer cell motility

Tai Kiuchi, Elena Ortiz-Zapater, James Monypenny, Daniel R. Matthews, Lan K. Nguyen, Jody Barbeau, Oana Coban, Katherine Lawler, Brian Burford, Daniel J. Rolfe, Emanuele de Rinaldis, Dimitra Dafou, Michael A. Simpson, Natalie Woodman, Sarah Pinder, Cheryl E. Gillett, Viviane Devauges, Simon P. Poland, Gilbert Fruhwirth, Pierfrancesco Marra, Ykelien L. Boersma, Andreas Plückthun, William J. Gullick, Yosef Yarden, George Santis, Martyn Winn, Boris N. Kholodenko, Marisa L. Martin-Fernandez, Peter Parker, Andrew Tutt, Simon M. Ameer-Beg,* Tony Ng*

*Corresponding author. E-mail: simon.ameer-beg@kcl.ac.uk (S.M.A.-B.); tony.ng@kcl.ac.uk (T.N.)

Published 19 August 2014, *Sci. Signal.* **7**, ra78 (2014)
DOI: 10.1126/scisignal.2005157

This PDF file includes:

Other Supplementary Material for this manuscript includes the following:
(available at www.sciencesignaling.org/cgi/content/full/7/339/ra78/DC1)

Movie S1 (.avi format). Migration of EGFR- and EGFP-expressing MCF-7 cells in an HB-EGF gradient.
Movie S2 (.avi format). Migration of ErbB4 CYT2 mICD–EGFP–expressing MCF-7 cells in an HB-EGF gradient.
Movies S3 and S4 (.avi format). Two examples of EGFR- and ErbB4 CYT2–expressing MCF-7 cells chemotaxing toward an HB-EGF gradient.

Text S1:

Development of a core model of the EGFR–ErbB4 CYT2 interaction network

We employed a modeling approach based on ordinary differential equations (ODE). The reaction rates were formulated generally at the elementary step level, using mass-action kinetic law. The kinetic scheme of the model is given in fig. S6A and a description of the model reactions, ODE equations and parameters is given in Table S1 and S2 below, based on which any reader can reproduce the model simulations. In addition, the *Mathematica* code of the model can be provided upon request. We chose to keep the model simple and base it on key biological observations captured by the data. Specifically, we made various important assumptions which are built into the model, as detailed below:

Experimental data shows that unliganded EGFR can also be internalized for degradation but at a 10-fold slower rate than EGF-stimulated receptor (85). Thus, for simplicity we assume that only the activated EGFR homodimer (pE11) can internalize and be degraded by Cbl.

Experimental evidence suggests that upon ligand stimulation, Cbl is recruited to the activated receptors (namely EGFR and ErbB4) via the adaptor protein Grb2 (86). For simplicity, we consider the Grb2-Cbl complex as a binding partner for the receptor and CYT2, denoted as GC in the kinetic scheme (fig. S6A).

We assume that ErbB4 CYT2 can bind phosphorylated EGFR (pE11) and unphosphorylated EGFR (E11) as well as the ligand-bound monomer form of EGFR (E-E1). However the alternative assumption where ErbB4 CYT2 only binds the dimer forms of EGFR also results in similar predictions of switch-like behaviours.

Following EGFR binding to CYT2, Cbl can bind CYT2-bound EGFR. Our data (Fig. 3F) show that in the resulting complex, Cbl does not trigger EGFR degradation efficiently. In fact, using a CYT2 mutant that does not bind Cbl, we observed at least 10-fold increase in EGFR degradation. Thus, because the putative

complex of CYT2-bound EGFR with Cbl would have a much lower degradation rate, we neglect this trimeric complex. Simulations show that including this complex in the model does not change the switch-like behavior of phosphorylated and total EGFR concentrations.

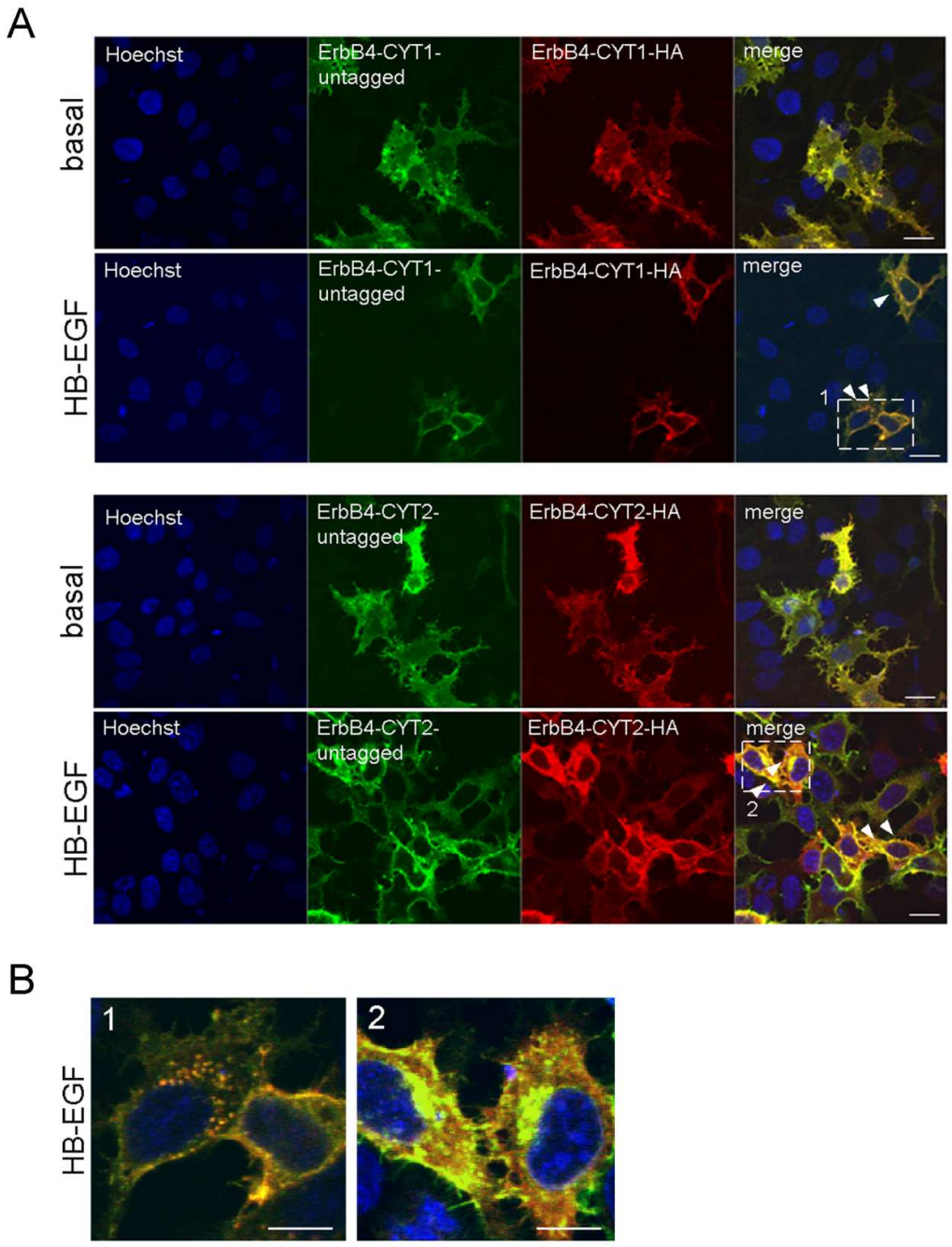

Supplementary Figure S1: Evaluation of the subcellular localization of tagged ErbB4 isoforms by immunofluorescence. (A) Immunostaining of untagged and

HA-tagged forms of exogenously expressed ErbB4 isoforms (upper panel: CYT1, lower panel: CYT2) in MCF-7 cells. After transfection with indicated plasmids cells were fixed and stained with anti-ErbB4 and anti-HA primary antibodies and Alexa 488-conjugated anti-rabbit and Cy3-conjugated anti-mouse secondary antibodies respectively. Cell nuclei were labeled with Hoescht 33342. Scale bar, 20 µm. (B) Enlargements of respective boxed regions (1 & 2) in A & B (Scale bar, 10 µm). Images are representative of 2 independent experiments.

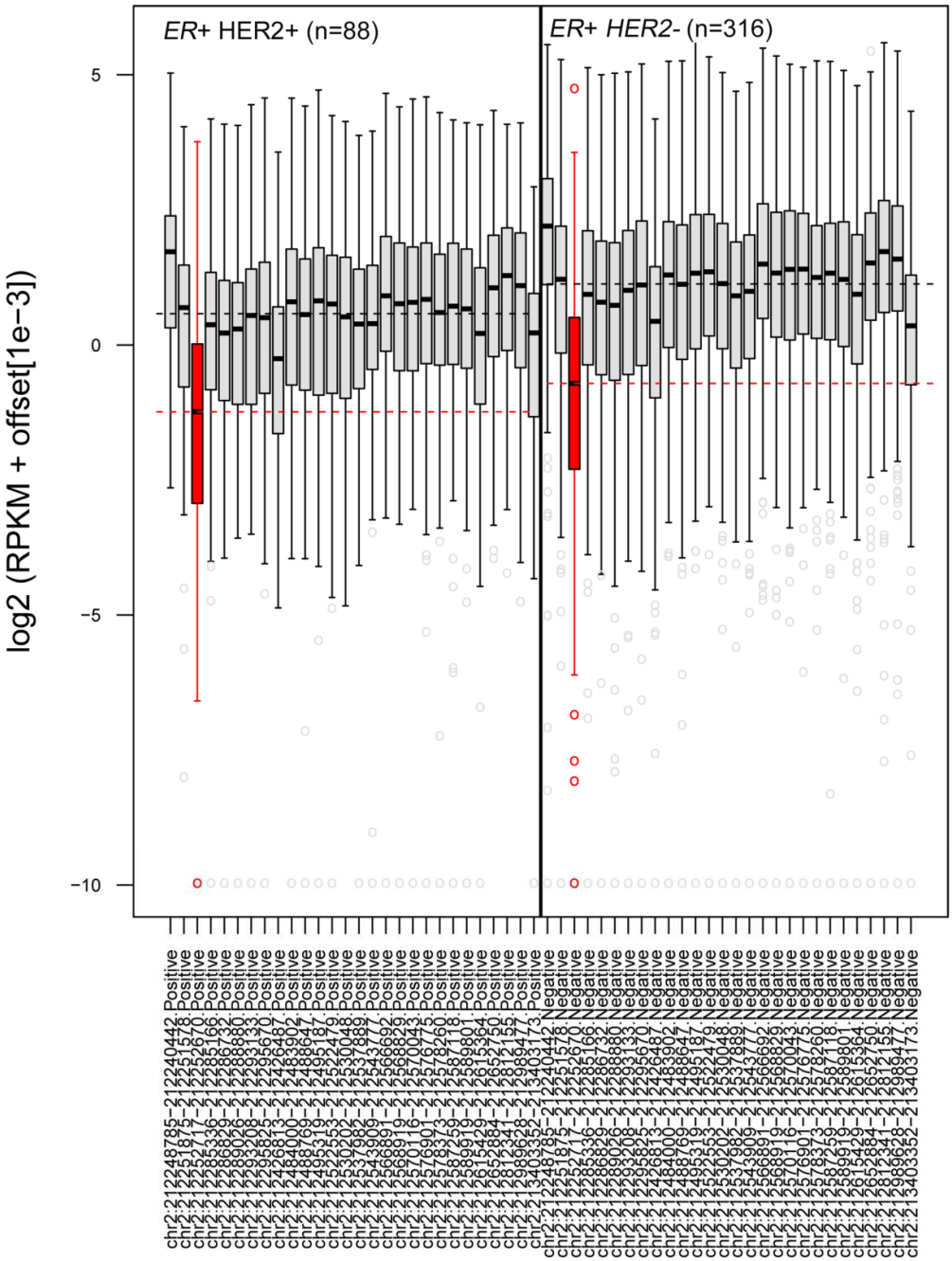

Supplementary Figure S2: Abundance of *ErbB4* exon–specific sequences in 404 human breast cancer samples within the TCGA RNASeq database. Boxplot of log2

reads per kilobase transcript per million reads (RPKM) values per exon (JMa isoform) for ER-positive samples, displayed according to HER2 status. Dotted lines show median RPKM for all exons except for the JMb-specific exon 15b (black; total *JMa* expression, *CYT1+CYT2*) and for exon26 only (red; *CYT1* specific). Comparison of median total (*CYT1+CYT2*) expression (black dotted lines) and median *CYT1* expression (red dotted lines) suggests an overall increase in relative *CYT2* expression in both ER+ HER2- samples and ER+ HER2+ patients.

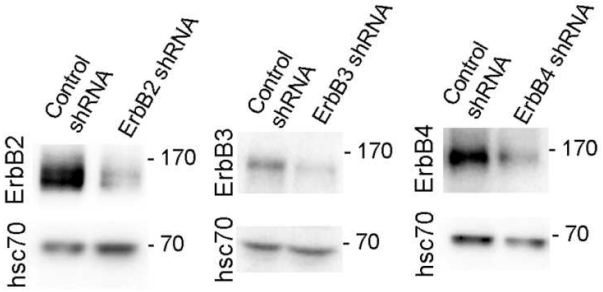

Supplementary Figure S3: The effect of knockdown of individual ErbB family members on EGF-dependent EGFR degradation. Lysates from MCF-7 cells stably transduced with lentivirus encoding non-targeting shRNA or ErbB2, ErbB3 or ErbB4 shRNA were blotted with the indicated antibodies. (N = 3 independent experiments.)

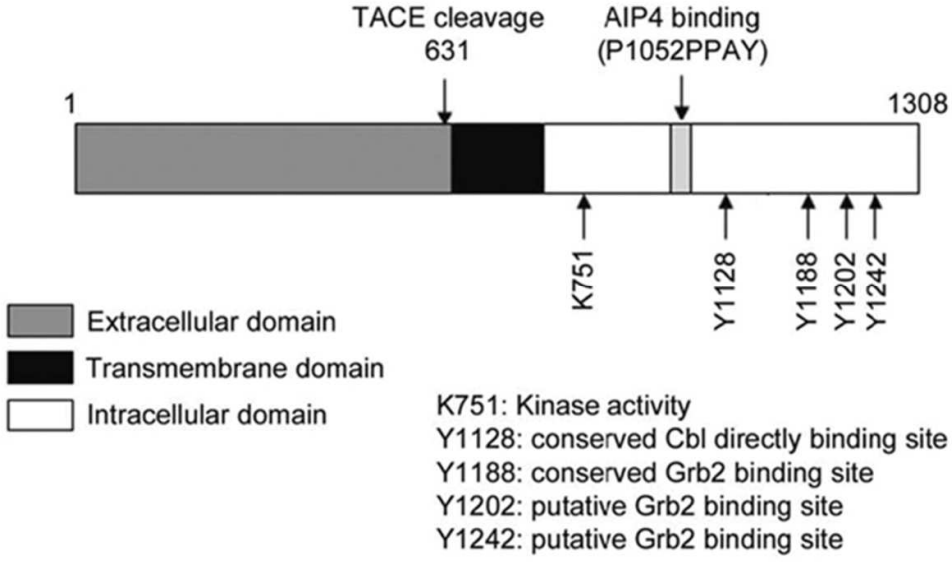

Supplementary Figure S4: Schematic of conserved and putative c-Cbl and Grb2 binding sites in ErbB4 JMa CYT1. Identified sites were used to design ErbB4 CYT2 truncation mutants to determine the region(s) important for c-Cbl recruitment.

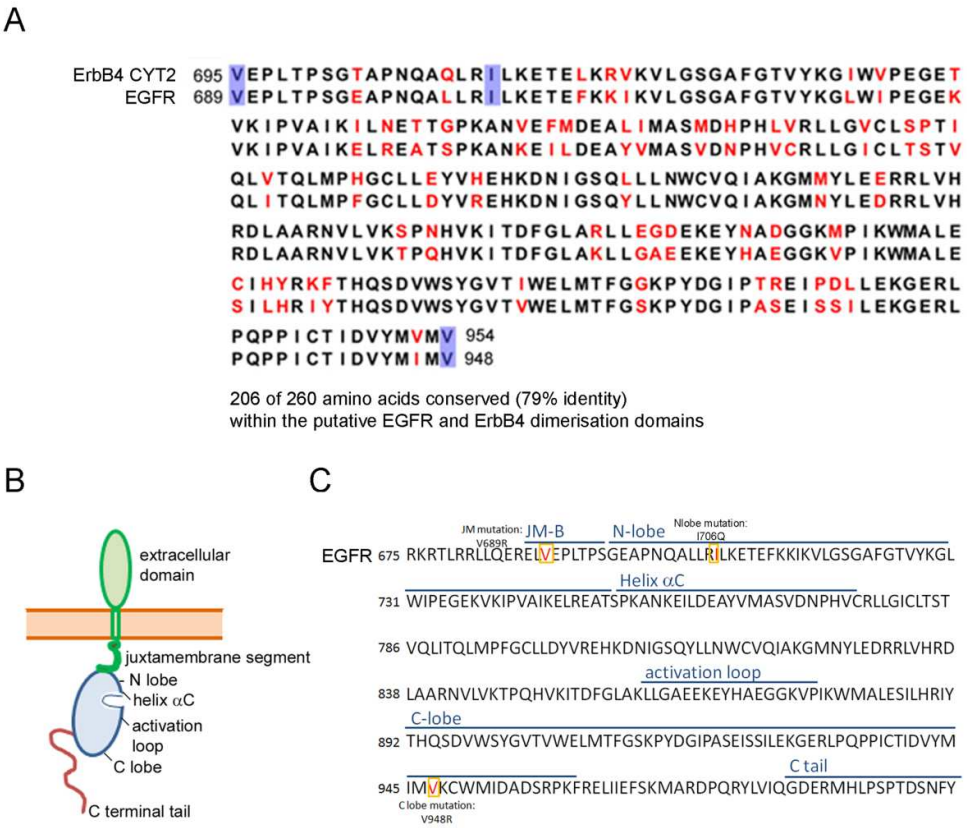

Supplementary Figure S5: Sequence homology alignment of the EGFR and ErbB4 CYT2 dimerization domains and associated residues targeted for mutagenesis. (A) Sequence homology alignment of the putative EGFR and ErbB4 CYT2 dimerization domains. Variations in the amino acid sequence are highlighted in red. (B) Schematic diagram of EGFR showing the different domains of the protein. (C) EGFR sequence highlighting location of introduced mutations (red).

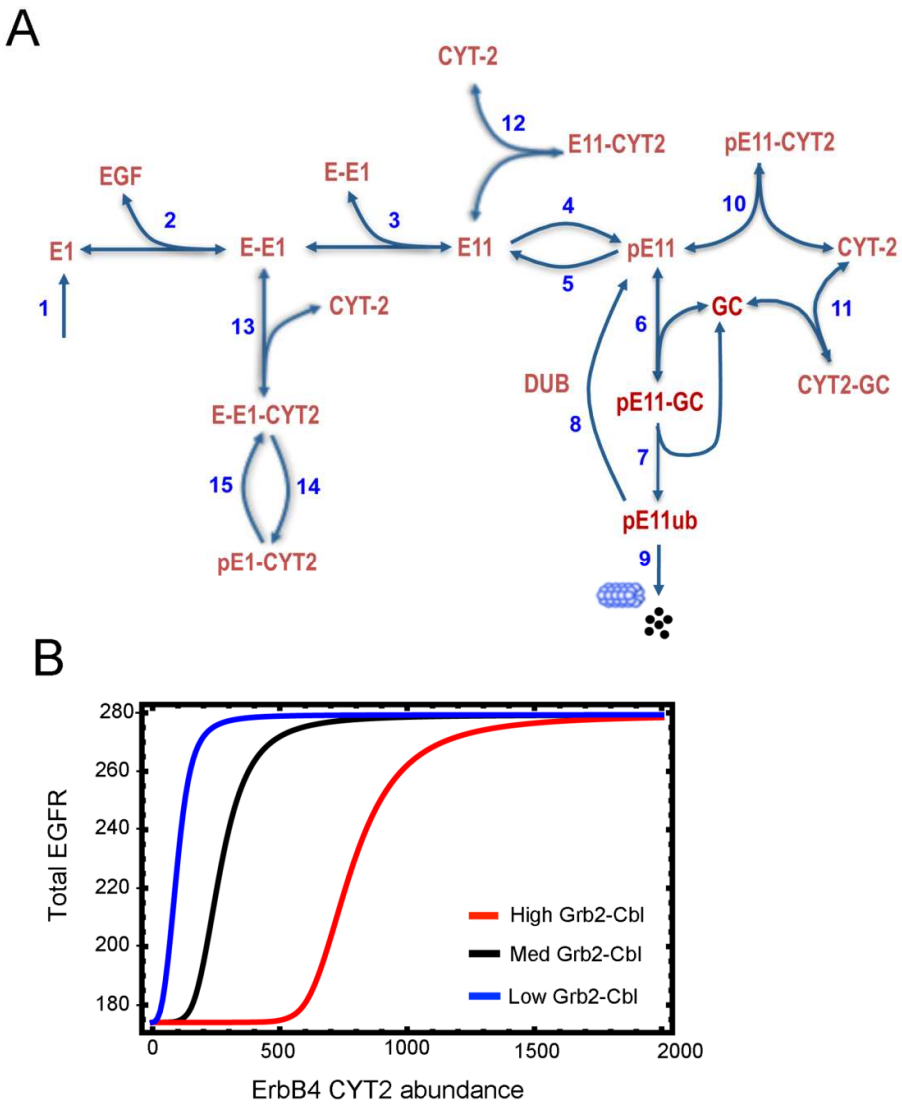

Supplementary Figure S6. Kinetic model of the core EGFR:ErbB4 CYT2 interaction network. (A) Kinetic scheme of the simplified EGFR:CYT2 interaction network model. The model development and description are presented in text S1. Abbreviation: E1 = EGFR, E-E1=EGF-EGFR, E11 = ligand bound EGFR dimer, pE11 = phosphorylated EGFR dimer, CYT2 = ErbB4 CYT2, GC = Grb2-c-Cbl, pE11ub =

ubiquitinated EGFR, DUB = Deubiquitinase. The reactions are numbered for ease of reference (see text S1). (B) Simulated steady-state dependence of the total EGFR on the ErbB4 CYT2 abundance at different concentrations (10, 100 and 500 nM) of the Grb2-c-Cbl complex (the units for the X- and Y-axis are in nM).

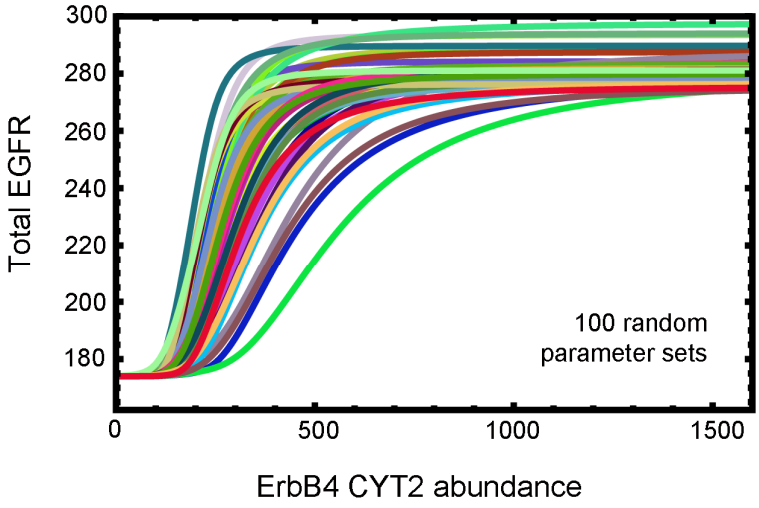

Supplementary Figure S7: Simulated steady-state concentrations of total EGFR over random parameter sets. The dependence of total EGFR on the abundance of ErbB4 CYT2 over multiple random parameter sets. 100 random parameter sets were generated within two-fold ranges of the reference set given in text S1, tables S1 and S2 (for example, within the ranges [p/2, 2×p] where p is the reference parameter value). Units for the X- and Y-axis are in nM.

Table S1. Reactions and reaction rates of the core EGFR–ErbB4 CYT2 interaction model. The first- (dissociation k_r, catalytic k_c, degradation k_d) and second-order (association k_f) rate constants are expressed in s^{-1} and nM^{-1} s^{-1}. Synthesis rate is expressed in nM s^{-1}. Model parameters are either measured or primarily based on our previous publication (87).

No	Reactions	Reaction rates	Parameter values	References
1	Ø → E1	**v1** = kf1	kf1=0.001	(88)
2	EGF + E1 ↔ EGF-E1	**v2** = kf2* [EGF]*[E1] – kr2*[EGF-E1]	kf2= 0.0001, kr2= 0.0175	(88)
3	EGF-E1 + EGF-E1 ↔ E11	**v3** = kf3* $[EGF\text{-}E1]^2$ – kr3*[E11]	kf3= 0.5005, kr3= 0.1717	(88)
4	E11 → pE11	**v4** = kc4* [E11]	kc4= 0.6496	(88)
5	pE11 → E11	**v5** = Vmax5* [pE11]/(Km5+ [pE11])	Vmax5=22 3 Km5=486	(88)
6	pE11 + GC ↔ pE11-GC	**v6** = kf6* [pE11]*[GC] – kr6*[pE11-GC]	kf6= 0.0097, kr6= 0.5737	(88)
7	pE11-GC → pE11ub + GC	**v7** = kc7* [pE11-GC]	kc7= 0.01	Estimated
8	pE11ub → pE11	**v8** = kc8* [pE11ub]	kc8= 0.001	Estimated
9	pE11ub → Ø	**v9** = kc9*[pE11ub]	kc9=	(88)

			0.0259	
10	pE11 + CYT2 ↔ pE11-CYT2	**v10** = kf10* [pE11]*[CYT2] – kr10*[pE11-CYT2]	kf10= 0.9 kr10= 1.33	(88) and measured in this study
11	CYT2 + GC ↔ CYT2-GC	**v11** = kf11* [CYT2]*[GC] – kr11*[CYT2-GC]	kf11= 0.05, kr11= 0.1	(88)
12	E11 + CYT2 ↔ E11-CYT2	**v12** = kf12* [E11]*[CYT2] – kr12*[E11-CYT2]	kf12= 0.9 kr12= 1.33	(88) and measured in this study
13	E-E1 + CYT2 ↔ E-E1-CYT2	**v13** = kf13* [E-E1]*[CYT2] – kr13*[E-E1-CYT2]	kf13= 0.9 kr13= 1.33	(88) and measured in this study
14	E-E1-CYT2→ pE1-CYT2	**v14** = kc14* [E-E1-CYT2]	kc14= 0.6496	(88)
15	pE1-CYT2→ E-E1-CYT2	**v15** = Vmax15* [pE1-CYT2]/(Km15+ [pE1-CYT2])	Vmax15=223 Km15=486	(88)

Table S2. Ordinary differential equations of the core EGFR–ErbB4 CYT2 interaction model. The reaction rates are given in table S1.

Left-hand Sides	Right-hand Sides	Initial	References
d[E1]/dt	v1 – v2	274	(88)
d[EGF/dt	– v2	100	Estimated
d[E-E1]/dt	v2 – v3 – v13	0	
d[E11]/dt	v3 – v4 + v5 – v12	0	
d[pE11]/dt	v4 – v5 – v6 + v8 –	0	
d[pE11-GC]/dt	v6 – v7	0	
d[pE11ub]/dt	v7 – v8 – v9	0	
d[GC]/dt	- v6 + v7 – v11	100	(88)
d[CYT2]/dt	– v10 – v11 – v12 –	400	(88)
d[pE11-CYT2]/dt	v10	0	
d[E11-CYT2]/dt	v12	0	
d[CYT2-GC]/dt	v7 – v11	0	
d[E-E1-CYT2]/dt	v13 – v14 + v15	0	
d[pE1-CYT2]/dt	v14 – v15	0	

Movie S1: Migration of EGFR- and EGFP-expressing MCF-7 cells in an HB-EGF gradient.

Time-lapse imaging of MCF-7 cells in the Dunn direct-viewing chemotaxis chamber. Cells were microinjected with EGFR & EGFP control vector 24 hours prior to filming. Left and right panels show sequentially acquired epifluorescence and phase-contrast images enabling the identification of microinjected cells. 250 ng/ml HB-EGF was placed in the outer well of the chamber as a chemoattractant source. Sequential epifluorescence and phase-contrast images were acquired every 10 min and the duration

of the film sequence is 9 hours.

Movie S2: Migration of ErbB4 CYT2 mICD–EGFP–expressing MCF-7 cells in an HB-EGF gradient.

Time-lapse imaging of MCF-7 cells in the Dunn direct-viewing chemotaxis chamber. Cells were microinjected with ErbB4 CYT2 mICD-EGFP vector 24 hours prior to filming. Left and right panels show sequentially acquired epifluorescence and phase-contrast images enabling the identification of microinjected cells. 250 ng/ml HB-EGF was placed in the outer well of the chamber as a chemoattractant source. Sequential epifluorescence and phase-contrast images were acquired every 10 min and the duration of the film sequence is 9 hours.

Movies S3 and S4: Two examples of EGFR- and ErbB4 CYT2–expressing MCF-7 cells chemotaxing towards an HB-EGF gradient.

Time-lapse imaging of MCF-7 cells in the Dunn direct-viewing chemotaxis chamber. Cells were microinjected with EGFR & EGFP-tagged ErbB4 CYT2 mICD 24 hours prior to filming. Left and right panels show sequentially acquired epifluorescence and phase-contrast images enabling the identification of microinjected cells. 250 ng/ml HB-EGF was placed in the outer well of the chamber as a chemoattractant source. Cells migrate collectively towards the outer well. Movie #4 shows an example of collective migration, or multicellular streaming, as a trailing cell migrates along the tail of a leading cell. Sequential epifluorescence and phase-contrast images were acquired every 10 min and the duration of each film sequence is 9 hours.